

# Artificial Super-Wettable Surfaces

Subjects: [Biochemical Research Methods](#)

Contributor: Sameer Hussain

Inspired by nature, significant research efforts have been made to discover the diverse range of biomaterials for various biomedical applications such as drug development, disease diagnosis, biomedical testing, therapy, etc. Polymers as bioinspired materials with extreme wettable properties, such as superhydrophilic and superhydrophobic surfaces, have received considerable interest in the past due to their multiple applications in anti-fogging, anti-icing, self-cleaning, oil–water separation, biosensing, and effective transportation of water. Apart from the numerous technological applications for extreme wetting and self-cleaning products, recently, super-wettable surfaces based on polymeric materials have also emerged as excellent candidates in studying biological processes.

[nature](#)[polymeric materials](#)[super-wettable surfaces](#)[bioinspired material](#)[biomedicine](#)

## 1. Extreme Wetting Surfaces Inspired by Nature and Their Applications in Biomedicine

For various biomedical uses, analysis, practical cell culture biomedical devices, and lab-on-one-chip systems may be used directly on bioinspired surfaces with intense weaving functionality. This segment provides new advances in the platforms that are bioinspired.

### 1.1. Cell Configuration for Studying Cellular Interactions

The topology and chemistry of surfaces are very dependent on protein adsorption and attachment to cells. With patterned superhydrophilic and superhydrophobic surfaces [\[1\]\[2\]\[3\]\[4\]\[5\]\[6\]\[7\]\[8\]\[9\]\[10\]\[11\]\[12\]](#), cell interactions have been thoroughly investigated. Piret et al. noted the selective adhesion of Chinese hamster ovary K1 cells to micropatterns on a surface of a superhydrophobic area [\[13\]](#). Likewise, Ishizak's research team demonstrated that physicochemical properties of surface (e.g., robustness, weight resistance) influence cell interactions and cell–cell adhesion [\[14\]](#). Specifically, the mouse 3T3 fibroblast cells adhered to the superhydrophilic areas immediately after seeding, while the cells scarcely adhered to superhydrophobic planes. The preference for protein absorption was due to the variation in cell attachment in superhydrophobic areas. The cultured cells modified their shapes and directions of adhesion selectively, based on the distance between superhydrophilic areas. Moreover, there was direct contact between cells in adjacent locations under a designated cell gap of 250  $\mu\text{m}$  cell–cell. In terms of tissue and organism growth in distinct but neighboring compartments, multiple-cell-type cultivation proved to be important for imitating and analyzing different biological actions, such as intercellular connectivity and cell signaling. Multiple cell patterning forms were applied to a porous, hydrophilic/hydrophobic boundary substratum by

Efremov et al. [7]. These hydrophilic substrates with a superhydrophobic border were developed in two stages: firstly, a hydrophilic nanoporous layer of the polymer was generated through a UV polymerization reaction. Afterward, the hydrophilic polymer coating was placed over a hydrophobic, photographic material. With a photomask, the UV was radiated again to make the superhydrophobic boundaries. The resulting surface was used in a reciprocal culture medium through pre-patterned cell co-cultivation for cell migration and signaling. The movement of MLTy-mCherry and HeLa-GFP cell lines through the thin, superhydrophobic periphery to different geometries was tracked within three days of co-culture. Cell movement was avoided by the thin boundary and could be utilized without intermingling to cultivate different types of cells correctly. At the same time, Wnt proteins were also used for the cell signaling process, a crucial class of proteins issued by the association of border areas. Precisely, the Wnt ligand was cultured that expressed zebrafish fibroblast Pac-2 cells that neighbored each pattern without direct cell interaction. In the tissue's extracellular space, the proteins migrated independently without any interaction with the cell. Interactions between cell–cell and cell–biomaterial on flat, 2D surfaces have been extensively studied, but experiments have been more useful in 3D, as micro-environments are best imitated in vivo [15][16][17][18][19]. In hydrophilic, patterned, superhydrophobic substrates between cells and polymers, Salgado et al. [20] analyzed 3D interactions. UV/ozone irradiation was carried out by a superhydrophobic PS substrate using a square-patterned photomask. By comparing wettability in several 3D hydrogel sizes, the hydrophilic patterns could be repositioned (**Figure 1a(i)**). Fibroblast, L929, and MC3T3-E1 pre-osteoblast cells were employed for testing 3D cell–hydrogel interactions. Among 24 various hydrogels, alginate (Alg) with various amounts of chitosan (Chi), hyaluronic acid (HA), gelatin (G), and collagen (Coll) were combined. The cytotoxicity of various compositions of hydrogel (total 24) was studied for 24 h (**Figure 1a**) and 5  $\mu$ L of cell-mixed polymer/crossline solutions was deposited on the substratum. Followed by cell cultivation for 24 h, all the materials were evaluated for cell quantification and cell viability and assessed for cell metabolic activity. The fluorescence imaging studies of live (green) and dead (red) cells in hydrogels, after 24 h of culture, are shown in **Figure 1b**. Dead cells were comparatively low in a 40% Alg containing HA/G mixture but high in a 40% Alg–Coll mixture. It was observed that, for L929 fibroblast cells, 70% of the Alg hydrogels containing HA and Coll and hydrogels containing Chi demonstrated high and low viability. For Coll- and HA-style hydrogels with 70% Alg, L929 cells were of high viability but with low compatibility. Additionally, even though the bone native tissue and pre-bone (osteoid) represent the most abundant protein structure, the presence of Coll enhanced pre-osteoblast cell viability.

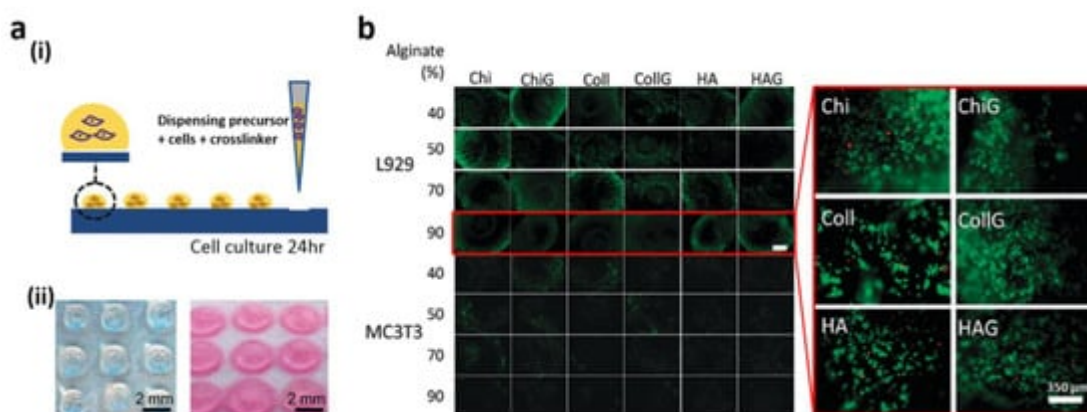


**Figure 1.** (a) (i) 3D hydrogel array of patterned hydrophilic marks; (ii) pictures before and after immersion in culture medium for 24 h; (b) fluorescence imaging of live (green) and dead (red) cells after cell culture for 24 h using 24 diverse hydrogels. Reprinted with permission from [20]. Copyright 2012 Oxford University Press.

## 1.2. Functional 3D Cell Spheroids

Cell culture in 3D conditions makes it possible to study interactions between the cell and extracellular matrix (ECM) more easily. Particularly, 3D cell spheroids offer cells with larger micro-environments in vivo [21][22]. Moreover, they also hold significant interest due to improved therapeutic capacities relative to cells grown on two-dimensional substrates. Traditionally, with classical dish cultivation, the hanging drop technique, and spinner flask culture [23][24][25][26], 3D cellular spheroids have been developed. By regulating their cell size and viability, hanging drop cultures can be associated with the hydrophilic patterned superhydrophobic surface [27][28][29]. Employing mussel-inspired adhesive polymer pDA [30], Lee et al. performed photolithography on the fluorosilane-coated superhydrophobic substrate to acquire the wettability-patterned surface. The hanging drop technique was employed for culturing rat islet cells (ICs) and human mesenchymal stem cells (MSCs) on the pDA-patterned surface. The active surface acquisition of 3D MSC spheroids increased the secretion of its vascular endothelial growth factor (VEGF) to an approximately 300% higher level compared to the level reached by the spinner flake culture. IC spheroids were also shown to improve glucose stimulus sensitivity by about 200%. In contrast with those cultivated with the technique of hanging drops on traditional Petri dishes, the uniformity, feasibility, and functionality of spheroid cells were increased. Such observations indicate that, by increasing cell–cell behavior, a spherical gout form increases cell–cell and cell–matrix interactions. Thus, it is helpful on superhydrophobic surfaces without hydrophilic architecture for hanging drop spheroid culture. The superhydrophobic, surface, 3D micro-environments dramatically decrease the cell cultivation media volume and avoid any soil contact. Neto and co-workers used a superhydrophobic surface patterned in micro-morphology for spheroid cultivation [13]. By applying force, the superhydrophobic surface of PS was primed and the surface was dented into sharp tips. Water droplets displayed a strong CA on the indentation as the water was fixed into the indentation. The preserved superhydrophobic features contributed to the creation of spherical water droplets on the surface and contact areas between the droplets and reduction of the surface. On the superhydrophobic surface of the mechanically modified PS, 3D spheroids were developed (**Figure 2a(i)**). Droplets-based cells continued, suspended from the indented base, despite the surface being rotated upside-down. Using different cell densities or drug concentrations, a cell spheroid combinatory study was performed and established using gravitational power. Mouse-immortalized lung fibroblast cell line L929 droplets were dispensed and cultured at two densities of thirty and forty thousand cells/droplet on the inverted superhydrophobic surface. The compound was subjected to varying levels of anti-cancer drug doxorubicin after 24 h of cell culture to determine the dose-dependent reaction of the tumor spheroid. In **Figure 2a(ii,iii)**, the results of drug screening achieved from the stained fluorescent images are demonstrated. The cell ratios in both spheroids between live (green) and dead (red) decreased as the dose decreased. Additionally, such ratios were larger at the lower density of spheroid. In comparison, dead cells collected mainly in the inner spheroid (**Figure 2a(iii)**) since it was more difficult to determine nutrients and waste releases in larger and denser spheroids.

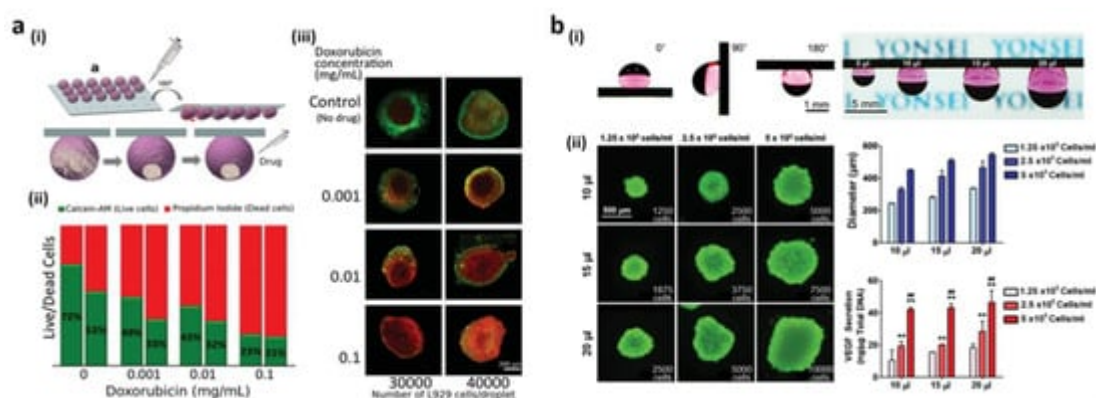


**Figure 2.** (a) (i) Sticking drop culture on a superhydrophobic surface with hollow shapes; (ii) the ratios of life (green) and dead (red) cells after introducing different doxorubicin concentrations; (iii) fluorescence imaging of L929 spheroids in doxorubicin-treated spheroids. (b) (i) Culture medium droplets on Si NWs coated with Pd and exposed with  $H_2$  at various tile angles; (ii) post four days of culture at different cell densities and medium sizes, live/dead cell staining, size distribution, and VEGF protein secretion from spheroids. ( $n = 3$ , \*\*:  $p < 0.01$  compared to the density of  $1.25 \times 10^5$  cells/mL, ###:  $p < 0.01$  compared to the density of  $2.5 \times 10^5$  cells/mL). Reprinted with permission from [13][31]. Copyright 2014 John Wiley and Sons.

The superhydrophobic surface with reversible adhesion properties was demonstrated by Seo et al. [24] to reduce cell–interface interactions during hanging drop spheroid culture. The gas-triggered adhesion to the hydrogen-sensitive surface of the superhydrophobic surface is shown in **Figure 3c,d** by deposition of Pd to Si NWs. Pd-coated Si NW arrays are adhesion swapping features that, using an attachment system without patterns, are specifically applied to 3D spheroid forming. The adhesion switch properties of Pd-coated Si NW arrays are directly applied to 3D spheroid formation using the hanging drop technique without any patterning process. Due the adhesion properties of Pd-coated Si NW arrays after exposure to  $H_2$ , droplets of variable sizes containing human adipose-derived stem cells (hADSC) were adhered and maintained under ambient air, as shown in **Figure 2b(i)**. **Figure 2b(ii)** indicates the viability of spheroids after four days of culture and the controllability of spheroid size by different cell densities ( $1.25$ ,  $2.5$ , and  $5.0 \times 10^5$  cells/mL) and different medium volumes ( $10$ ,  $15$ , and  $20\mu\text{L}$ ). It was demonstrated that the secretion of VEGF from hADSC spheroids depended on the size of the spheroids. Improved cell density paracrine behavior and culture medium volume adaptation were observed in hADSC spheroids. A decreased distribution and substantially improved VEGF secretions of hADSC spheroids were observed relative to traditional spinner bottles and Petri dishes. In contrast to the Petri-dish strategies, this drop-out strategy increased the efficacy of hADSC, paracrine seclusion, mitochondrial metabolic processes, apoptosis, and ECM. Additionally, an angiogenic potential was assessed as an operative assay for hADSC spheroids. The conditioned media obtained in Pd-coated Si NW pads from hADSC spheroids increased the proliferation of human endothelial cells and accelerated capacity formation.

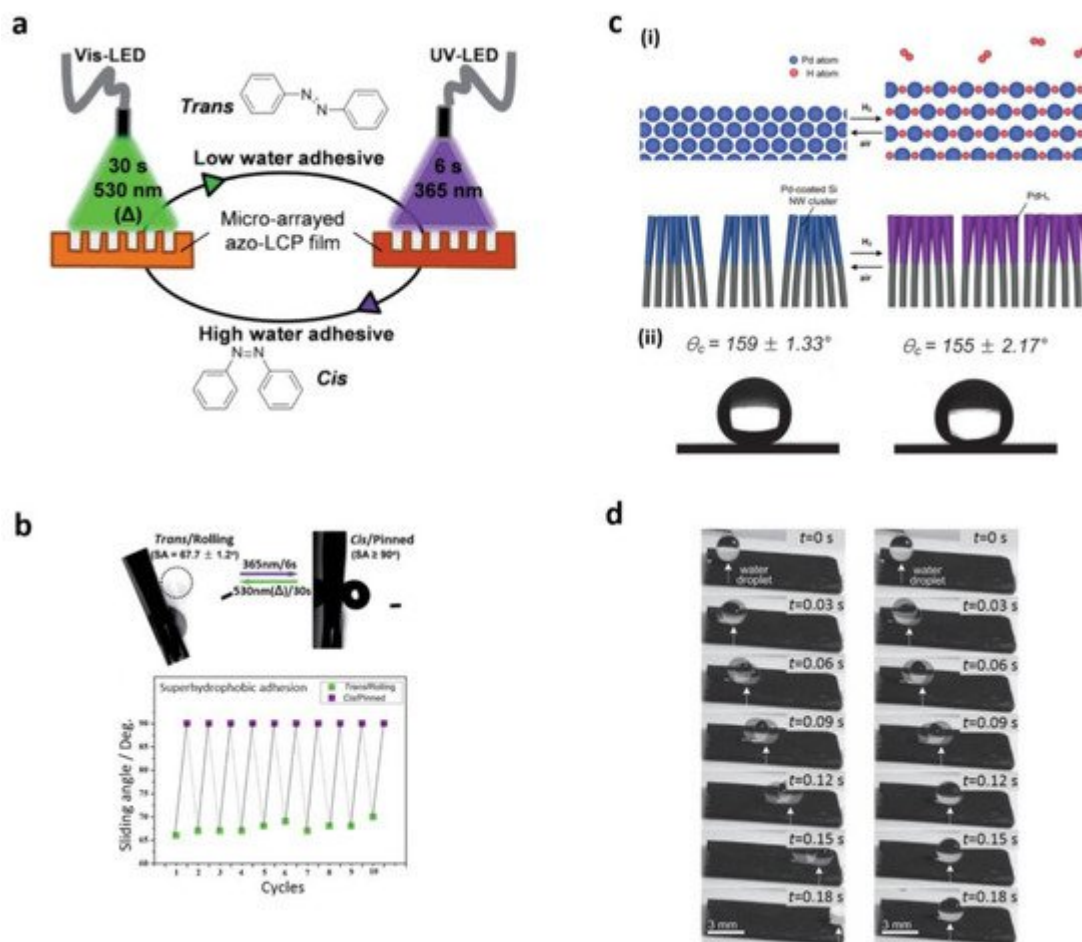


**Figure 3.** (a) Photoswitchable adhesion with UV and visible light excitation; (b) dynamic adhesion capability of LCP film; (c) (i) the volume of Pd layers deposited expanded on arrays of Si NWs under air and hydrogen atmosphere, (ii) the angles of contact confirming superhydrophobicity under similar conditions; (d) pictures of moving water droplets under similar conditions. Reprinted with permission from [107,108]. Copyright 2012 the Royal Chemical Society (RSC) and copyright 2013 John Wiley and Sons.

### 1.3. Biomedical Devices

In clinical applications for implantable biomedical instruments, the adhesion of harmful biomedical materials to the surface must be avoided. Thus, if the implanted system requires prevention of inflammation or infection in cell/tissue culture systems, an antibacterial surface property is highly desirable. Different methods for the development of antibacterial surfaces have been reported [32][33][34][35][36][37][38][39][40][41]. A superhydrophobic surface inspired by biological structures has become a favorable antibacterial surface due to the anti-fouling capability that could circumvent surface bacteria from adhering [42][43][44][45][46]. Privett et al. [42] also produced xerogels which contained silica colloids, fluoroalkoxysilane, and silane backbone. The superhydrophobic characteristics of the coated surface of the xerogel were facilitated by fluorinated silica nanoparticles for low surface energy and a hierarchical structure. The antibacterial properties of the xerogel were described by a conventional cell flow assay using Gram-negative *Pseudomonas aeruginosa* (*P. aeruginosa*) and Gram-positive *Staphylococcus aureus* (*S. aureus*). Microbial adhesion to the superhydrophobic xerogel surface was decreased by

98% and 99% relative to the blank area. The antibacterial properties of surfaces with Gram-negative bacteria were reported by Feschauf et al. [47], using superhydrophobic polycarbonate (PC) and polyethylene (PE) and PS substrates. Using a basic casting method, the superhydrophobic PC, PE, and PS surfaces were acquired from a micro/nanostructured PDMS casting. A total of 10  $\mu\text{L}$  of *E. coli* was cultured to test standardized PS, PC, and PE surface anti-bacterial properties. Then, a bacterial *E. coli* solution was cultivated for 24 h (**Figure 4**). Fewer than 100 colony-forming units (CFUs) were observed on PS- and PE-based superhydrophobic surfaces after 24 h, whereas no bacterial growth was observed on the PC substrate. Moreover, 100 CFUs were observed each for flat PS and PC, while 25,800 were observed for PE. These findings suggest that, relative to flat surfaces, superhydrophobic surfaces efficiently reduce adhesion of bacteria to <0.1%. Because of the wide variety of anti-fouling properties, liquid slippery surfaces often have tremendous potential for various medical applications in comparison to different liquids and environmental pressures. Over a wide range of temperatures, heats, surface tensions, and multiple conditions they retain repellency [46]. Epstein's research team [48] showed the importance of a slippery surface to avert binding biofilm. On a smooth, slippery surface, the bacteria were presented, which could not be anchored on the mobile interface compared to solid interface. Irrespective of the principal solid, porous structure, separate biofilm accumulations were stopped by a slippery surface over more than a week. In contrast to common, polyethylene glycol, anti-fouling surfaces, it also decreased bacterial attachment by 96–96.6%. To minimize the morbidity and mortality caused by thrombosis, Leslie et al. [49] used slippery properties on tubing and catheters of indwelling medical devices. They developed a tethered perfluorocarbon coating (TP) at the top of the tube followed by its coating with a liquid perfluorodecalin (LP) surface to attain anti-thrombogenic and non-adhesive surfaces. The thin, moving liquid layer permitted the tethered-liquid perfluorocarbon (TLP) surface to resist fluids effectively also after the surface contacted an immiscible liquid, such as blood (**Figure 4b(i)**). The surface was cleaned almost immediately from a new, whole human droplet of blood (**Figure 4b(ii)**). Compared to the uncoated surfaces of acrylic and polysulfone, they showed (**Figure 4c(i)**) a decrease in the adhesion and polymerization of the TLP surface. The slithery condition also decreased the adhesion of platelets in contrast to uncoated surfaces. These findings demonstrated that the smooth surface decreased fibrin polymerization and inhibited adherence, as well as plates activation. To realize an arteriogenic shunt for in vivo analysis of the anti-thrombogenic effect of the slippery surface, polycarbonate connectors, TLP-treated polyurethane cannulae, and medicinal, polyvinyl chloride (PVC)-based heart pulmonary perfusion tubes were studied. Compared with control tubes, **Figure 4c(ii)** displays polymer TLP-treated tubes that minimize occlusive thrombosis post flow for 8 h. Such noteworthy, anti-fouling properties can, therefore, be used in several additional applications.

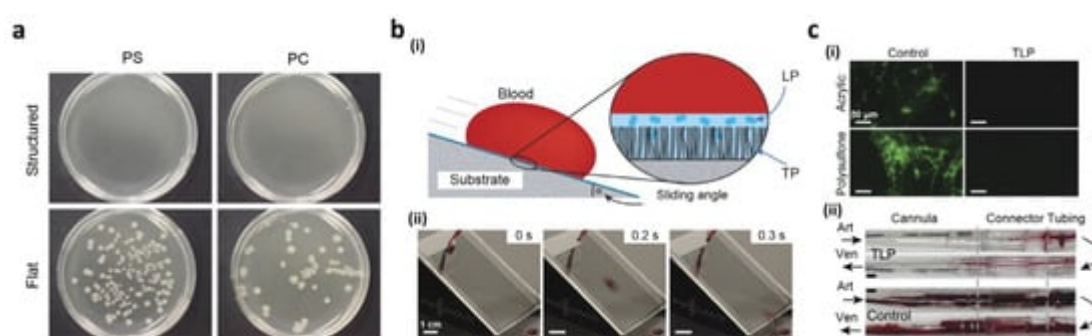


**Figure 4.** (a) The growth of bacteria on structured and smooth PS and PC substrates; (b) (i) the smooth surfaces after coating with tethered-liquid perfluorocarbon (TLP) showing blood repellency; (ii) the images of the slippery surface showing slipping of a blood droplet; (c) (i) fluorescence images of fibrinogen on polysulfone or acrylic surfaces in the presence and absence of TLP coating; (ii) the images of polycarbonate connectors, polyurethane cannulae, and PVC tubing in the presence and absence of TLP coating. Reproduced from [47] under CC BY license. Reprinted with permission from [49]. Copyright 2014 Nature Publishing Group.

## 1.4. Lab-on-a-Chip Based on Open Channel Droplets

In terms of fast penetration into the sample fluid, energy consumption and low samples, quick chemical and biological reactions [50][51][52][53][54][55][56][57][58][59][60], such as microfluidic droplet systems, have many advantages compared to traditional closed-channel, microfluidic applications. A gout-based microfluidic system [52] was introduced on a superhydrophobic, porous oxide membrane by You et al. To direct the water droplets, they inserted hydrophilic PDAs on superhydrophobic surfaces. A square pDA for more complex droplet handling was also planned in the middle of the pDA micro-line. A fluid droplet traveled along the micro-lines by momentum, stopping at the square, which showed adequate surface energy to catch the droplet. Such an immobilized droplet was pushed downwards by inserting a second droplet. With this droplet capacity to combine, preparation of monodispersed gold nanoparticles and rapid, structural protein changes were introduced. For chemical and biological organic solvent-based reactions and experiments, however, superhydrophobic hydrophilic patterned surfaces could not be employed. For compatibility with different solvents, a pDA, micropatterned slippery surface was introduced by You et al. [61]. To attain a fluid-guiding feature, PDA micro-lines were engineered on a nanostructured surface before lubricant infiltration. Multiple solvents, for example, gasoline, dimethyl sulfoxide, water, dimethylformamide, 1,2-dichloroethane, *n*-hexane, toluene, acetone, and diesel oils, were compatible with the produced slippery device. Any solvent with a surface tension larger than that of the lubricant could be depleted by gravitational force along the micro-lines by the infused lubricant located on top of the pDA micro-line. They implemented the square shape pattern for the gout mixture in the pDA micro-line intersection with the same aforementioned process (Figure 5a(i)) [52]. The chemical reactions using an organic solvent were carried out on the slippery surface of the pDA micro-model due to the broad compatibility of solvents. The organic reaction was performed between benzaldehyde and ortho-phenylenediamine to create 2-arylbenzimidazole. The droplet of THF solution composed of two reactants, as well as a THF, was dropped on the oily surface, as shown in Figure 5a(ii). By fast and homogeneous mixing, the reaction rate (70.3%) improved relative to the standard bulk reaction using a vial (52.1%). Furthermore, the surface was cleared and used again after ultrasonication.

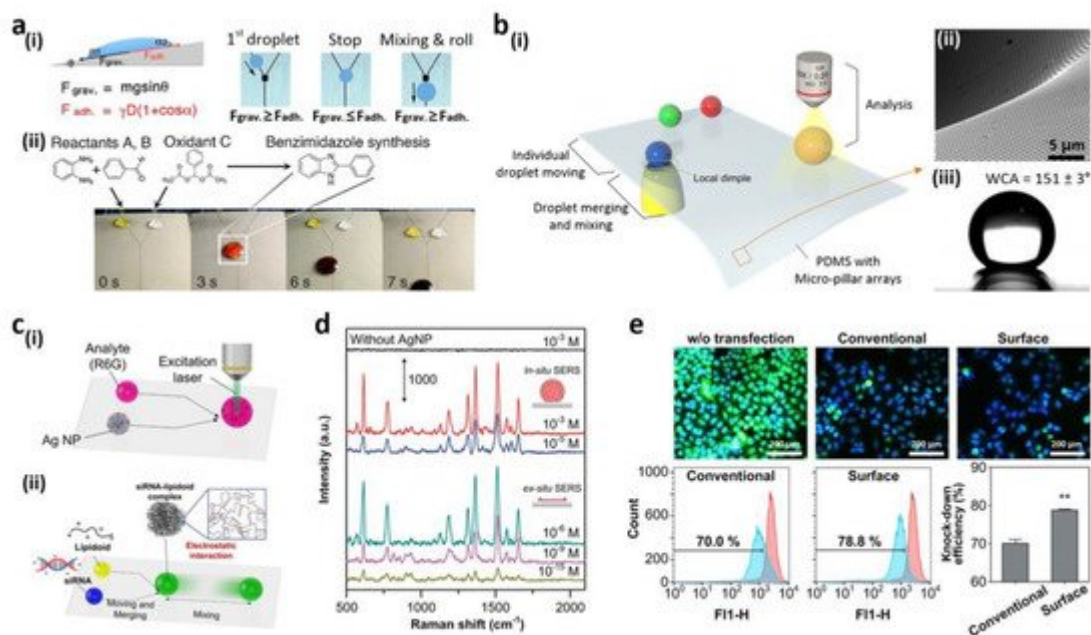


**Figure 5.** (a) (i) The movement of the droplet and its mixing on a slippery system fabricated with pDA (ii) THF-based chemical reaction on the slippery surface; (b) (i) regulation of motions of water (movement, mixing, and examination) on PDMS substrate appended with micropillar arrays; (ii) the dimple structure's SEM picture; (iii) water droplet image on the substrate of PDMS; (c) (i) the measurement system for SERS; (ii) formation of minor, interfering lipidoid-RNA complex; (d) SERS measurement spectra (in situ/ex situ) for R6G/Ag NP droplet mixture and an evaporated R6G/Ag NP droplet; (e) fluorescence imaging and flow cytometry studies of transfected GFP-Hela cells. Scale bar-200  $\mu\text{m}$  ( $n = 3$ ,  $** p < 0.01$ , compared to the conventional group). Reprinted with permission from [61][62]. Copyright 2014 American Chemical Society (ACS) and copyright 2015 Nature Publishing Group.

Decorated droplet-handling systems only had minimal control over fluid processes, for instance, start and stop motion. Newly developed by Seo et al., the superhydrophobic PDMS substrate contained micropillar arrays for programmed water droplet manipulation (Figure 5b(i)) [62]. When applying the substrate, the vacuum pressure on the suspended PDMS substratum was expanded (Figure 5b(ii)) to form a local, pale structure. Decreased performance and superhydrophobicity of the micropillar array was observed (Figure 5). In the interface region between the substrate and water droplets, the dimple arrangement could be used to monitor the motions of water droplets individually. The curvature was positive at the boundary of the pillars adjacent to the PDMS, and the width was greater than the flat substratum distance. The lower number of micropillars decreased the adhesiveness of the water and allowed isolation from the droplet substratum. The flow of water drops on the substratum also could not be conveniently regulated through the vacuum dimple structure; however, the moving direction could also be readily built without any additional pattern. Surface-enhanced Raman spectroscopy (SERS) analyzed the substrate's analytical efficiency (Figure 5c(i)). Rhodamine 6G (R6G) in situ/ex situ SERS tests were carried out at different concentrations (Figure 5d). In situ, individual water droplets consisting of Ag nanoparticles and R6G molecules were determined by the SERS and combined at the Raman detection point before the collection of data. The lower limit of detection for R6G/Ag NP was calculated to be  $10^{-5}$  M, owing to disseminated R6G and Ag molecules in a mixed droplet. The mixture was evaporated and its components condensed to resolve this detection

cap within an area of a certain length. The R6G molecules were also observed at  $10^{-15}$  M because of the aggregation of Ag NPs and R6G for ex situ SERS calculation. To manufacture regular, intracellular, gene transfer nanoparticles, they used the platform. In the lipid (ND98) complexes with green fluorescent protein (GFP) siRNA, a basic method of mixing and blending outlets was used (siGFP). On the platform, homogenous mixing of droplets and the efficiency of transfections to GFP-HeLa cells from the platform's lipidoid-siRNA complexes ( $78.8\% \pm 0.5\%$ ), in contrast to classical manual pipetting mixing (70.0%), could be achieved, as shown in **Figure 5e**.

## 1.5. Fluorescent Intelligence Sensing Based on Bioinspired Super-Wettable Patterns

In analytical chemistry, fluorescence is a popular detection method. In a light-absorption process, fluorescence is a luminescence process induced by an appropriate molecule under light excitation. Fluorescence intensity is measurable at specific excitation/emission wavelengths. Under dilute concentrations, the amplitude of fluorescence would be equal to the fluorophore concentration. Several groups recently focused their efforts on the fabrication of bioinspired super-wettable microchips for profound fluorescence-based detection. These examples will be highlighted in the following text: mainly their features such as anchoring and enriching capabilities for biosensing. The analytes were stored in microdroplets that were enclosed inside the superhydrophilic microwells with the superhydrophobic substrate serving as a wall to keep the microdroplets from spreading. Huang and co-workers recorded sensitive detection of metal ions by integrating the fluorescence technique, as seen in **Figure 6a**, by using the anchoring capacities of bioinspired micro-patterns. A hydrophilic, photonic-crystal, colloidal microchip was created by assembling hydrophilic, photonic-crystal, colloidal particles on a hydrophilic–hydrophobic patterned substrate. The developed microchip improved fluorescence detection in multiple channels selectively, as well as performed highly effective testing under discriminative conditions using twelve metal ions [63]. Such a well-performing, patterned microchip demonstrates a modern use of bioinspired microchips in detection and their crucial role in the development of sophisticated fluorescent devices and advanced discriminative analysis.

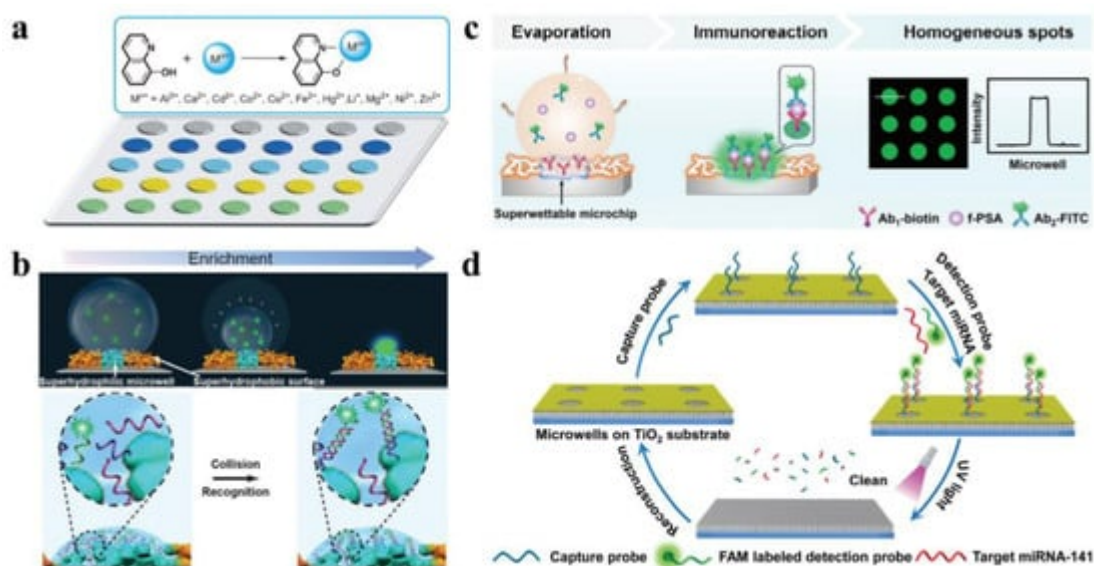


**Figure 6.** Super-wettable fluorescence finding. (a) High-performance metal-ion recognition using a bioinspired photonic-crystal microchip; (b) ultra-trace DNA identification using super-wettable microchips; (c) example of free prostate-specific antigen (f-PSA) detection on homogeneous super-wettable microchips in a schematic diagram; (d) a green super-wettable miRNA biochip built on TiO<sub>2</sub> substrate. Reprinted with permission from [63][64][65][66]. Copyright 2013, 2015 Wiley-VCH and copyright 2018 Elsevier B.V.

The “analyte solution concentration in the hydrophilic region increases as the microdroplet evaporates, which is ideal for capturing the analyte for ultra-trace detection. In **Figure 6b** [64], ultra-trace fluorescent DNA detection is demonstrated by using the super-wettable microchips’ enrichment ability. UV-based etching of the octadecyl trichlorosilane (OTS), functionalized, superhydrophobic, nanodendritic Si coating through a photomask and deposition of candle soot were employed to create this super-wettable microchip. The analyte was captured from an extremely diluted solution by constant evaporation and emission signals were eventually intensified to attain the recognition of DNA with a low detection limit ( $10^{-16}$  M). Aggregation-induced emission enhancement (AIEE) and evaporation-induced enhancement were accomplished concurrently by incorporating AIE molecules onto a super-wettable microchip [64]. As a result of the synergetic enhancement, a miRNA biosensor with enhanced efficiency (detection limit-1 pM, linear range- $10^{-6}$  to  $10^{-12}$  M) can be achieved. The super-wettable microchip’s overall fluorescence strength was just half that of industrial hydrophilic or hydrophobic glass substrates. Due to the coffee rings, however, unequal signal propagation occurred on the hydrophilic and hydrophobic surfaces, possibly limiting repeatability. The sensitive and precise identification of biomarkers included excellent spots in the superhydrophilic microwells. The coffee-ring effect could be reduced in super-wettable microchips, and the homogeneity of superhydrophilic spots could be increased, as seen in **Figure 6c** [65]. The superior Marangoni effect in the superhydrophilic spot and the reduced outward flow, owing to the large hydrodynamic flow resistance of 3D Si nanodendritic structure, contributed to this phenomenon. **Figure 6d** [66][67][68] displays the sustainable super-wettable biochips for miRNA identification. The nanodendritic TiO<sub>2</sub> nanostructure was made hydrothermally on FTO-coated glass substrates, then modified with OTS and exposed to UV light via a photomask. By using its anchoring and enrichment abilities, super-wettable fluorescence detection provides a sensitive technique that could be especially useful in biomarker sampling, diagnosis, and disease monitoring. However, the need for large instruments and complicated biomolecule fluorescent labeling can restrict their use in point-of-care (PoC) detection. Integration of bioinspired micropatterns with compact fluorescence instruments for point-of-care research will be a potential priority.

Aside from the above-discussed papers, recent years have witnessed several other polymeric-materials-based, super-wettable surfaces for applications in diverse research areas [69][70][71][72][73][74][75][76][77][78]. To summarize, some common polymeric-material-based, super-wettable surfaces utilized for various applications are illustrated in **Table 1**.

**Table 1.** Some common polymeric materials used in the fabrication of super-wettable surfaces.

Polymeric Materials	Fabrication Method	Application	Wetting Property	Reference
Hyaluronic acid (HA)	Phase separation	Tissue engineering	Hydrophobic	Ref <a href="#">[20]</a>
Polyethylene (PE)	Shrink-induced mold method	Antibacterial	Superhydrophobic	Ref <a href="#">[47]</a>
Polycarbonate (PC)	Shrink-induced mold method	Antibacterial	Superhydrophobic	Ref <a href="#">[47]</a>
Polystyrene (PS)	Electrohydrodynamics (EHD)	Tissue engineering	Superhydrophobic	Ref <a href="#">[79]</a>
1H,1H,2H,2H-perfluoro-decyl trichlorosilane (PFDTs)	Wet chemical self-assembly	Conductive stainless steel	Superhydrophobic	Ref <a href="#">[80]</a>
Poly(vinyl alcohol) (PVA)	Solvent evaporation	Petal effects	Hydrophilic-Superhydrophobic	Ref <a href="#">[81]</a>
Poly(p-xylylene) (PPX)	Soft lithography	Self-cleaning	Superhydrophobic	Ref <a href="#">[82]</a>
Polydimethyl siloxane (PDMS)	Soft lithography	Water adhesion	Hydrophilic-Superhydrophobic	Ref <a href="#">[82]</a>
Polydopamine (PD)	Soft lithography	Water adhesion	Hydrophilic-Superhydrophobic	Ref <a href="#">[82]</a>
Polytetrafluoroethylene (PTFE)	Sol-gel strategy	Water adhesion	Superhydrophobic	Ref <a href="#">[69]</a>
Polyvinylpyrrolidone (PVP)	Sol-gel strategy	Self-cleaning	Superhydrophobic	Ref <a href="#">[69]</a>
Polyamide (PA)	Dip-coating method	Water and oil separation	Superhydrophobic	Ref <a href="#">[74]</a>
Silane-modified polymer (SMP)	Spray-coating method	Water and oil separation	Superhydrophobic	Ref <a href="#">[74]</a>

## References

- Geyer, F.; Ueda, E.; Liebel, U.; Grau, N.; Levkin, P. Superhydrophobic-superhydrophilic micropatterning: Towards genome-on-a-chip cell microarrays. *Angew. Chem. Int. Ed.* 2011, 50, 8424–8427.
- Piret, G.; Galopin, E.; Coffinier, Y.; Boukherroub, R.; Legrand, D.; Slomianny, C. Culture of mammalian cells on patterned superhydrophilic/superhydrophobic silicon nanowire arrays. *Soft*

- Matter 2011, 7, 8642–8649.
3. Alves, N.M.; Shi, J.; Oramas, E.; Santos, J.; Tomás, H.; Mano, J.F. Bioinspired superhydrophobic poly(l-lactic acid) surfaces control bone marrow derived cells adhesion and proliferation. *J. Biomed. Mater. Res. A* 2009, 9, 480–488.
  4. Oliveira, S.M.; Song, W.; Alves, N.M.; Mano, J.F. Chemical modification of bioinspired superhydrophobic polystyrene surfaces to control cell attachment/proliferation. *Soft Matter* 2011, 7, 8932–8941.
  5. Ballester Beltran, J.; Rico, P.; Moratal, D.; Song, W.; Mano, J.F. Role of superhydrophobicity in the biological activity of fibronectin at the cell-material interface. *Soft Matter* 2011, 7, 10803–10811.
  6. Auad, P.; Ueda, E.; Levkin, P.A. Facile and multiple replication of superhydrophilic-superhydrophobic patterns using adhesive tape. *ACS Appl. Mater. Interfaces* 2013, 5, 8053–8057.
  7. Efremov, A.N.; Stanganello, E.; Welle, A.; Scholpp, S.; Levkin, P.A. Micropatterned superhydrophobic structures for the simultaneous culture of multiple cell types and the study of cell-cell communication. *Biomaterials* 2013, 34, 1757–1763.
  8. Oliveira, S.M.; Alves, N.M.; Mano, J.F. Cell interactions with superhydrophilic and superhydrophobic surfaces. *J. Adhes. Sci. Technol.* 2014, 28, 843–863.
  9. Li, H.; Yang, Q.; Li, G.; Li, M.; Wang, S.; Song, Y. Splitting a droplet for femtoliter liquid patterns and single cell isolation. *ACS Appl. Mater. Interfaces* 2015, 7, 9060–9065.
  10. Galopin, E.; Piret, G.; Szunerits, S.; Lequette, Y.; Faille, C.; Boukherroub, R. Selective adhesion of bacillus cereus spores on heterogeneously wetted silicon nanowires. *Langmuir* 2010, 26, 3479–3484.
  11. Dar, A.A.; Hussain, S.; Dutta, D.; Iyer, P.K.; Khan, A.T. One-pot synthesis of functionalized 4-hydroxy-3-thiomethylcoumarins: Detection and discrimination of  $\text{Co}^{2+}$  and  $\text{Ni}^{2+}$  ions. *RSC Adv.* 2015, 5, 57749–57756.
  12. Marcon, L.; Addad, A.; Coffinier, Y.; Boukherroub, R. Cell micropatterning on superhydrophobic diamond nanowires. *Acta Biomater.* 2013, 9, 4585–4591.
  13. Neto, A.I.; Correia, C.R.; Custódio, C.A.; Mano, J. Biomimetic miniaturized platform able to sustain arrays of liquid droplets for high-throughput combinatorial tests. *Adv. Funct. Mater.* 2014, 24, 5096–5103.
  14. Ishizaki, T.; Saito, N.; Takai, O. Correlation of cell adhesive behaviors on superhydrophobic superhydrophilic and micropatterned superhydrophobic/superhydrophilic surfaces to their surface chemistry. *Langmuir* 2010, 26, 8147–8154.
  15. Minchinton, A.I.; Tannock, I.F. Drug penetration in solid tumours. *Nat. Rev. Cancer* 2006, 6, 583–592.

16. Pampaloni, F.; Reynaud, E.G.; Stelzer, E.H.K. The third dimension bridges the gap between cell culture and live tissue. *Nat. Rev. Mol. Cell Biol.* 2007, 8, 839–845.
17. Frith, J.E.; Thomson, B.; Genever, P.G. Dynamic three-dimensional culture methods enhance mesenchymal stem cell properties and increase therapeutic potential. *Tissue Eng. Part C Methods* 2010, 16, 735–749.
18. Meli, L.; Jordan, E.T.; Clark, D.S.; Linhardt, R.J.; Dordick, J.S. Influence of a three-dimensional, microarray environment on human cell culture in drug screening systems. *Biomaterials* 2012, 33, 9087–9096.
19. Breslin, S.; Driscoll, L. Three-dimensional cell culture the missing link in drug discovery. *Drug Discov. Today* 2013, 18, 240–249.
20. Salgado, C.L.; Oliveira, M.B.; Mano, J.F. Combinatorial cell-3D biomaterials cytocompatibility screening for tissue engineering using bioinspired superhydrophobic substrates. *Integr. Biol.* 2012, 4, 318–327.
21. Tofilon, P.J.; Buckley, N.; Deen, D.F. Effect of cell-cell interactions on drug sensitivity and growth of drug-sensitive and -resistant tumor cells in spheroids. *Science* 1984, 226, 862–864.
22. Bartosh, T.J.; Ylöstalo, J.H.; Mohammadipoor, A.; Bazhanov, N.; Coble, K.; Claypool, K.; Lee, R.H.; Choi, H.; Prockop, D.J. Aggregation of human mesenchymal stromal cells (MSCs) into 3D spheroids enhances their antiinflammatory properties. *Proc. Natl. Acad. Sci. USA* 2010, 107, 13724–13729.
23. Torisawa, Y.; Takagi, A.; Nashimoto, Y.; Yasukawa, T.; Shiku, H.; Matsue, T. A multicellular spheroid array to realize spheroid formation, culture, and viability assay on a chip. *Biomaterials* 2007, 28, 559–566.
24. Brophy, C.M.; Luebke-Wheeler, J.; Amiot, B.P.; Khan, H.; Remmel, R.P.; Rinaldo, P.; Nyberg, S.L. Rat hepatocyte spheroids formed by rocked technique maintain differentiated hepatocyte gene expression and function. *Hepatology* 2009, 49, 578–586.
25. Hsiao, A.Y.; Torisawa, Y.; Tung, Y.C.; Sud, S.; Taichman, R.S.; Pienta, K.J.; Takayama, S. Microfluidic system for formation of pc-3 prostate cancer co-culture spheroids. *Biomaterials* 2009, 30, 3020–3027.
26. Wong, S.F.; No, D.Y.; Choi, Y.Y.; Kim, D.S.; Chung, B.G.; Lee, S.H. Concave microwell based size-controllable hepatosphere as a three-dimensional liver tissue model. *Biomaterials* 2011, 32, 8087–8096.
27. Lin, R.Z.; Chang, H.Y. Recent advances in three-dimensional multicellular spheroid culture for biomedical research. *Biotechnol. J.* 2008, 3, 1172–1184.

28. Tung, Y.C.; Hsiao, A.Y.; Allen, S.G.; Torisawa, Y.; Ho, M.; Takayama, S. High-throughput 3D spheroid culture and drug testing using a 384-hanging drop array. *Analyst* 2011, 136, 473–478.
29. Cavnar, S.P.; Salomonsson, E.; Luker, K.E.; Luker, G.D.; Takayama, S. Transfer, imaging, and analysis plate for facile handling of 384 hanging drop 3D tissue spheroids. *J. Lab. Autom.* 2014, 19, 208–214.
30. Lee, M.; Yang, K.; Hwang, Y.H.; Byun, Y.; Lee, D.Y.; Cho, S.W.; Lee, H. Spheroform: Therapeutic spheroid-forming nanotextured surfaces inspired by desert beetle *Physosterna cribripes*. *Adv. Healthc. Mater.* 2015, 4, 511–515.
31. Seo, J.; Lee, J.S.; Lee, K.; Kim, D.; Yang, K.; Shin, S.; Mahata, C.; Jung, H.B.; Lee, W.; Cho, S.W.; et al. Switchable water-adhesive, superhydrophobic palladium-layered silicon nanowires potentiate the angiogenic efficacy of human stem cell spheroids. *Adv. Mater.* 2014, 26, 7043–7050.
32. Heinonen, S.; Huttunen Saarivirta, E.; Nikkanen, J.P.; Raulio, M.; Priha, O.; Laakso, J.; Storgårds, E.; Levänen, E. Antibacterial properties and chemical stability of superhydrophobic silver-containing surface produced by sol-gel route. *Colloids Surf. A Physicochem. Eng. Asp.* 2014, 453, 149–161.
33. Wang, Z.; Ou, J.; Wang, Y.; Xue, M.; Wang, F.; Pan, B.; Li, C.; Li, W. Anti-bacterial superhydrophobic silver on diverse substrates based on the mussel-inspired polydopamine. *Surf. Coat. Technol.* 2015, 280, 378–383.
34. Heinonen, S.; Nikkanen, J.P.; Laakso, J.; Raulio, M.; Priha, O.; Levänen, E. Bacterial growth on a superhydrophobic surface containing silver nanoparticles. *IOP Conf. Ser. Mater. Sci. Eng.* 2013, 47, 012064.
35. Berendjchi, A.; Khajavi, R.; Yazdanshenas, M. Fabrication of superhydrophobic and antibacterial surface on cotton fabric by doped silica-based sols with nanoparticles of copper. *Nanoscale Res. Lett.* 2011, 6, 594.
36. Wu, M.; Ma, B.; Pan, T.; Chen, S.; Sun, J. Silver-nanoparticle-colored cotton fabrics with tunable colors and durable antibacterial and self-healing superhydrophobic properties. *Adv. Funct. Mater.* 2016, 26, 569–576.
37. Khalil-Abad, M.S.; Yazdanshenas, M.E. Superhydrophobic antibacterial cotton textiles. *J. Colloid Interface Sci.* 2010, 351, 293–298.
38. Zhang, L.; Zhang, L.; Yang, Y.; Zhang, W.; Lv, H.; Yang, F.; Lin, C.; Tang, P. Inhibitory effect of super-hydrophobicity on silver release and antibacterial properties of super-hydrophobic Ag/TiO<sub>2</sub> nanotubes. *J. Biomed. Mater. Res. Part B Appl. Biomater.* 2016, 104, 1004–1012.
39. Lichter, J.A.; Van Vliet, K.J.; Rubner, M.F. Design of antibacterial surfaces and interfaces: Polyelectrolyte multilayers as a multifunctional platform. *Macromolecules* 2009, 42, 8573–8586.

40. Song, K.; Gao, A.; Cheng, X.; Xie, K. Preparation of the superhydrophobic nano-hybrid membrane containing carbon nanotube based on chitosan and its antibacterial activity. *Carbohydr. Polym.* 2015, 130, 381–387.
41. Yang, H.; You, W.; Shen, Q.; Wang, X.; Sheng, J.; Cheng, D.; Cao, X.; Wu, C. Preparation of lotus-leaf-like antibacterial film based on mesoporous silica microcapsule-supported Ag nanoparticles. *RSC Adv.* 2014, 4, 2793–2796.
42. Privett, B.J.; Youn, J.; Hong, S.A.; Lee, J.; Han, J.; Shin, J.H.; Schoenfish, H. Antibacterial fluorinated silica colloid superhydrophobic surfaces. *Langmuir* 2011, 27, 9597–9601.
43. Fadeeva, E.; Truong, V.K.; Stiesch, M.; Chichkov, B.N.; Crawford, R.; Wang, J.; Ivanova, E.P. Bacterial retention on superhydrophobic titanium surfaces fabricated by femtosecond laser ablation. *Langmuir* 2011, 27, 3012–3019.
44. Liu, T.; Dong, L.; Liu, T.; Yin, Y. Investigations on reducing microbiologically influenced corrosion of aluminum by using super-hydrophobic surfaces. *Electrochim. Acta* 2010, 55, 5281–5285.
45. Ye, W.; Shi, Q.; Hou, J.; Jin, J.; Fan, Q.; Wong, S.; Xu, X.; Yin, J. Superhydrophobic coating of elastomer on different substrates using a liquid template to construct a biocompatible and antibacterial surface. *J. Mater. Chem. B* 2014, 2, 7186–7191.
46. Grinthal, A.; Aizenberg, J. Mobile interfaces, Liquids as a perfect structural material for multifunctional, antifouling surfaces. *Chem. Mater.* 2014, 26, 698–708.
47. Freschauf, L.R.; McLane, J.; Sharma, H.; Khine, M. Shrink-induced superhydrophobic and antibacterial surfaces in consumer plastics. *PLoS ONE* 2012, 7, e40987.
48. Epstein, A.K.; Wong, T.S.; Belisle, R.A.; Boggs, E.M.; Aizenberg, J. Liquid-infused structured surfaces with exceptional anti-biofouling performance. *Proc. Natl. Acad. Sci. USA* 2012, 109, 13182–13187.
49. Leslie, D.C.; Waterhouse, A.; Berthet, J.; Valentin, T.M.; Watters, A.L.; Jain, A.; Kim, P.; Hatton, B.D.; Nedder, A.; Donovan, K.; et al. A bioinspired omniphobic surface coating on medical devices prevents thrombosis and biofouling. *Nat. Biotechnol.* 2014, 32, 1134–1140.
50. Balu, B.; Berry, A.D.; Hess, D.W.; Breedveld, V. Patterning of superhydrophobic paper to control the mobility of micro-liter drops for two-dimensional lab-on-paper applications. *Lab Chip* 2009, 9, 3066–3075.
51. Mertaniemi, H.; Jokinen, V.; Sainiemi, L.; Franssila, S.; Marmur, A.; Ikkala, O.; Ras, R.H.A. Superhydrophobic tracks for low-friction, guided transport of water droplets. *Adv. Mater.* 2011, 23, 2911–2914.
52. You, I.; Kang, S.M.; Lee, S.; Cho, Y.O.; Kim, J.B.; Lee, S.B.; Nam, Y.S.; Lee, H. Polydopamine microfluidic system toward a two-dimensional, gravity-driven mixing device. *Angew. Chem. Int.*

- Ed. 2012, 51, 6126–6130.
53. Sousa, M.P.; Mano, J.F. Superhydrophobic paper in the development of disposable labware and lab-on-paper devices. *ACS Appl. Mater. Interfaces* 2013, 5, 3731–3737.
  54. Elsharkawy, M.; Schutzius, T.M.; Megaridis, C.M. Inkjet patterned superhydrophobic paper for open-air surface microfluidic devices. *Lab Chip* 2014, 14, 1168–1175.
  55. Zhao, Y.; Xu, Z.; Niu, H.; Wang, X.; Lin, T. Magnetic liquid marbles, Toward “lab in a droplet”. *Adv. Funct. Mater.* 2015, 25, 437–444.
  56. Kim, D.; Seo, J.; Shin, S.; Lee, S.; Lee, K.; Cho, H.; Shim, W.; Lee, H.; Lee, T. Reversible liquid adhesion switching of superamphiphobic Pd-decorated Ag dendrites via gas-induced structural changes. *Chem. Mater.* 2015, 27, 4964–4971.
  57. Jonsson Niedziolka, M.; Lapierre, F.; Coffinier, Y.; Parry, S.J.; Zoueshtiagh, F.; Foat, T.; Thomy, V.; Boukherroub, R. EWOD driven cleaning of bioparticles on hydrophobic and superhydrophobic surfaces. *Lab Chip* 2011, 11, 490–496.
  58. Lapierre, F.; Piret, G.; Drobecq, H.; Melnyk, O.; Coffinier, Y.; Thomy, V.; Boukherroub, R. High sensitive matrix-free mass spectrometry analysis of peptides using silicon nanowires-based digital microfluidic device. *Lab Chip* 2011, 11, 1620–1628.
  59. Lapierre, F.; Harnois, M.; Coffinier, Y.; Boukherroub, R.; Thomy, V. Split and flow: Reconfigurable capillary connection for digital microfluidic devices. *Lab Chip* 2014, 14, 3589–3593.
  60. Li, L.; Breedveld, V.; Hess, D.W. Hysteresis controlled water droplet splitting on superhydrophobic paper. *Colloid Polym. Sci.* 2013, 291, 417–426.
  61. You, I.; Lee, T.G.; Nam, Y.S.; Lee, H. Fabrication of a micro-omnifluidic device by omniphilic/omniphobic patterning on nanostructured surfaces. *ACS Nano* 2014, 8, 9016–9024.
  62. Seo, J.; Lee, S.K.; Lee, J.; Seung, L.J.; Kwon, H.; Cho, S.W.; Ahn, J.H.; Lee, T. Path-programmable water droplet manipulations on an adhesion controlled superhydrophobic surface. *Sci. Rep.* 2015, 5, 12326.
  63. Huang, Y.; Li, F.; Qin, M.; Jiang, L.; Song, Y. A multi-stopband photonic-crystal microchip for high-performance metal-ion recognition based on fluorescent detection. *Angew. Chem. Int. Ed. Engl.* 2013, 52, 7296–7299.
  64. Xu, L.P.; Chen, Y.; Yang, G.; Shi, W.; Dai, B.; Li, G.; Cao, Y.; Wen, Y.; Zhang, X. Ultratrace DNA Detection Based on the Condensing-Enrichment Effect of Superwettable Microchips. *Adv. Mater.* 2015, 27, 6878–6884.
  65. Chen, Y.; Xu, L.P.; Meng, J. Superwettable microchips with improved spot homogeneity toward sensitive biosensing. *Biosens. Bioelectron.* 2018, 102, 418–424.

66. Wu, T.; Xu, T.; Chen, Y.; Yang, Y.; Xu, L.; Zhang, X.; Wang, S. Renewable superwettable biochip for miRNA detection. *Sens. Actuators B* 2018, 258, 715–721.
67. Chen, X.; Liu, C.; Xu, Z.; Pan, Y.; Liu, J.; Du, L. An effective PDMS microfluidic chip for chemiluminescence detection of cobalt (II) in water. *Microsyst. Technol.* 2012, 19, 99–103.
68. Sima, F.; Xu, J.; Wu, D.; Sugioka, K. Ultrafast laser fabrication of functional biochips: New avenues for exploring 3D micro- and nano-environments. *Micromachines* 2017, 8, 40.
69. He, J.; Zhao, Y.; Yuan, M.; Hou, L.; Abbas, A.; Xue, M.; Ma, X.; He, J.; Qu, M. Fabrication of durable polytetrafluoroethylene superhydrophobic materials with recyclable and self-cleaning properties on various substrates. *J. Coat. Technol. Res.* 2020, 17, 755–763.
70. He, J.; Zhang, Y.; Zhou, Y.; Wang, J.; Zhao, Y.; Ma, L.; Abbas, A.; Qu, M. A facile approach to fabricate the durable and buoyant superhydrophobic fabric for efficient oil/water separation. *Fibers Polym.* 2019, 20, 1003–1010.
71. Stetsyshyn, Y.; Raczkowska, J.; Budkowski, A.; Awsiuk, K.; Kostruba, A.; Nastyshyn, S.; Harhay, K.; Lychkovskyy, E.; Ohar, H.; Nastishin, Y. Cholesterol-based grafted polymer brushes as alignment coating with temperature-tuned anchoring for nematic liquid crystals. *Langmuir* 2016, 32, 11029–11038.
72. Pan, Z.; Cheng, F.; Zhao, B. Bioinspired polymeric structures with special wettability and their applications. *Polymers* 2017, 9, 725.
73. Raczkowska, J.; Stetsyshyn, Y.; Awsiuka, K.; Lekkac, M.; Marzec, M.; Harhay, K.; Ohar, H.; Ostapiv, D.; Sharand, M.; Yaremchuk, I.; et al. Temperature-responsive grafted polymer brushes obtained from renewable sources with potential application as substrates for tissue engineering. *Appl. Surf. Sci.* 2017, 407, 546–554.
74. Zhang, T.; Wang, S.; Huang, J.; Jin, Y.; Zhao, G.; Zhang, C.; Li, C.; Yu, J.; Jia, Y.; Jiao, F. Facile fabrication of versatile superhydrophobic coating for efficient oil/water separation. *J. Dispers. Sci. Technol.* 2021, 42, 363–372.
75. Wang, R.; Wu, F.; Yu, F.; Zhu, J.; Gao, X.; Jiang, L. Anti-vapor-penetration and condensate microdrop self-transport of superhydrophobic oblique nanowire surface under high subcooling. *Nano Res.* 2021, 14, 1429–1434.
76. Wang, D.; Sun, Q.; Hokkanen, M.J.; Zhang, C.; Lin, F.-Y.; Liu, Q.; Zhu, S.-P.; Zhou, T.; Chang, Q.; He, B.; et al. Design of robust superhydrophobic surfaces. *Nature* 2020, 582, 55–59.
77. Zeng, J.; Zhang, Y.; Zeng, T.; Aleisa, R.; Qiu, Z.; Chen, Y.; Huang, J.; Wang, D.; Yan, Z.; Yin, Y. Anisotropic plasmonic nanostructures for colorimetric sensing. *Nano Today* 2020, 32, 100855.
78. Xu, T.; Xu, L.-P.; Zhang, X.; Wang, S. Bioinspired superwettable micropatterns for biosensing. *Chem. Soc. Rev.* 2019, 48, 3153–3165.

79. Jiang, L.; Zhao, Y.; Zhai, J. A lotus-leaf-like superhydrophobic surface: A porous microsphere/nanofiber composite film prepared by electrohydrodynamics. *Angew. Chem. Int. Ed.* 2004, 116, 4438–4441.
80. Li, Y.; Huang, X.J.; Heo, S.H.; Li, C.C.; Choi, Y.K.; Cai, W.P.; Cho, S.O. Superhydrophobic bionic surfaces with hierarchical microsphere/SWCNT composite arrays. *Langmuir* 2007, 23, 2169–2174.
81. Feng, L.; Zhang, Y.; Xi, J.; Zhu, Y.; Wang, N.; Xia, F.; Jiang, L. A superhydrophobic state with high adhesive force. *Langmuir* 2008, 24, 4114–4119.
82. Kang, S.M.; You, I.; Cho, W.K.; Shon, H.K.; Lee, T.G.; Choi, I.S. One-step modification of superhydrophobic surfaces by a mussel-inspired polymer coating. *Angew. Chem. Int. Ed.* 2010, 49, 9401–9404.

---

Retrieved from <https://encyclopedia.pub/entry/history/show/43500>